Revealing Excitonic Phonon Coupling in (PEA)2(MA)n-1PbnI3n+1 2D Layered Perovskites

Joanna M Urban, Gabriel Chehade, Mateusz Dyksik, Matan Menahem, Alessandro Surrente, Gaëlle Trippé-Allard, Duncan Kennedy Maude, Damien Garrot, Omer Yaffe, Emmanuelle Deleporte, et al.

Revealing Excitonic Phonon Coupling in $(PEA)_2(MA)_{n-1}Pb_nI_{3n+1}$ 2D Layered Perovskites

Joanna M. Urban,[†,‡] Gabriel Chehade,[‡] Mateusz Dyksik,[†,¶] Matan Menahem,[§] Alessandro Surrente,[†] Gaëlle Trippé-Allard,[‡] Duncan K. Maude,[†] Damien Garrot,[‖] Omer Yaffe,[§] Emmanuelle Deleporte,[‡] Paulina Plochocka,[*,†,¶] and Michal Baranowski[*,†,¶]

†*Laboratoire National des Champs Magnétiques Intenses, UPR 3228, CNRS-UGA-UPS-INSA, Grenoble and Toulouse, France*

‡*Université Paris-Saclay, ENS Paris-Saclay, CNRS, CentraleSupelec, LuMIn, 91405 Orsay, France*

¶*Department of Experimental Physics, Faculty of Fundamental Problems of Technology, Wroclaw University of Science and Technology, Wroclaw, Poland*

§*Department of Materials and Interfaces Weizmann Institute of Science Rehovoth 76100, Israel*

‖*Groupe d'Etude de la Matière Condensée, Université de Versailles Saint-Quentin-en-Yvelines, Université Paris-Saclay, 45 Avenue des Etats-Unis, 78035, Versailles, France*

E-mail: paulina.plochocka@lncmi.cnrs.fr; michal.baranowski@pwr.edu.pl

Abstract

The family of 2D Ruddlesden-Popper perovskites is currently attracting great interest of the scientific community as highly promising materials for energy harvesting and light emission applications. Despite the fact that these materials are known for decades, only recently has it become apparent that their optical properties are driven by the exciton-phonon coupling which is controlled by the organic spacers. However, the detailed mechanism of this coupling, which gives rise to complex absorption and emission spectra, is the subject of ongoing controversy. In this work we show that the particularly rich, absorption spectra of $(PEA)_2(CH_3NH_3)_{n-1}Pb_nI_{3n+1}$, (where PEA stands for phenylethylammonium and $n = 1, 2, 3$), are related to a vibronic progression of excitonic transition. In contrast to other two dimensional perovskites we observe a coupling to a high energy (40 meV) phonon mode probably related to the torsional motion of the NH_3^+ head of the organic spacer.

Low-dimensional layered metal-halide perovskites have recently attracted attention as a significantly more stable alternative[1–4] to their 3D counterparts which suffer from rapid degradation in air.[5] These natural quantum wells, consisting of octahedral slabs separated by large organic spacers, are considered promising candidates for energy harvesting applications[1,4,6–9] and light-emitting devices.[10–13]

The most intensively studied members of 2D perovskite family are those of the 2D Ruddlesden-Popper (RP) type that are described by the formula $(R_1NH_3)_2B_{n-1}Pb_nI_{3n+1}$[13–15] where n is the number of perovskite octahedra in the inorganic slab, R_1NH_3 is the large organic molecule which forms the barriers and B is a smaller cation, for example Cs, methylammonium ($CH_3NH_2^+$) or formamidinium ($CH(NH_2)_2^+$). The hydrophobic-

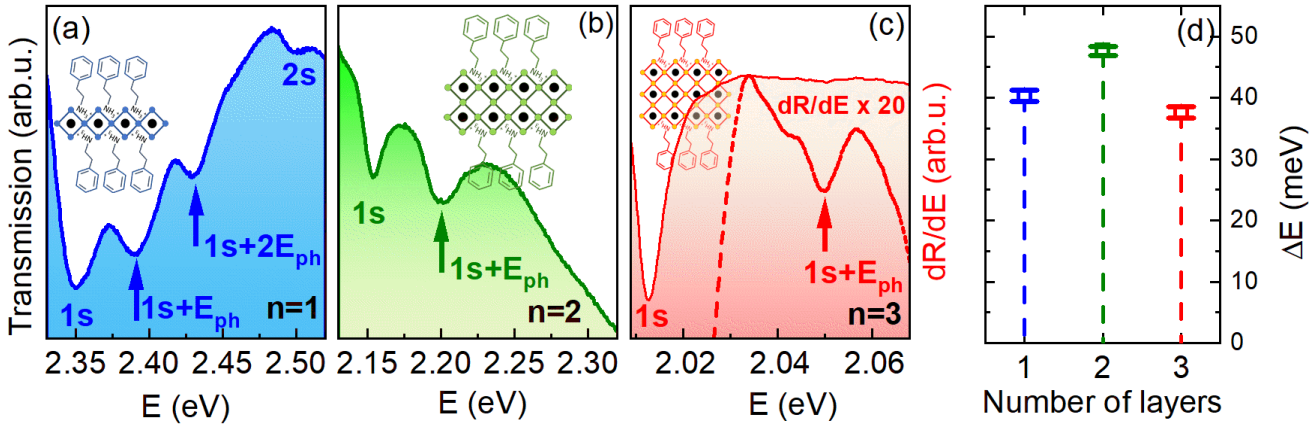

Figure 1: Transmission spectra of (a) $n = 1$ and (b) $n = 2$ thin film samples at $T = 4\,\mathrm{K}$. (c) First derivative of the reflectivity spectrum for the $n = 3$ sample. The dashed line in this panel shows the same derivative spectrum in a higher energetic range magnified $\times 20$ and shifted to fit the figure scale to highlight the feature around 2.05 eV. The arrows mark features assigned to phonon replicas of the 1s excitonic transition. (d) Energetic separation of the 1s transition and the first replica phonon replica (marked by arrows in (a)-(c)) as a function of the number of layers. The error bars correspond to the standard deviations of the mean values obtained from fitting spectra for all magnetic fields acquired from several shots.

ity of the spacer molecules is the main cause of the strongly improved stability of 2D perovskites.[4,13] The 2D confinement provided by the band alignment of the inorganic and organic part of RP perovskites, together with dielectric confinement (due to the contrasting dielectric constants of barriers and octahedral slab), result in very strong excitonic effects.[14–17] The exciton binding energy can reach several hundreds of meV,[16,18–21] which is detrimental for the application of RP perovskites as solar cells absorbers[1,4,7] and beneficial in the case of light emitters[22,23] and polaritonic devices operating at room temperature.[10,24] The enhanced excitonic effects, characteristic of many other 2D semiconductors,[25–29] is accompanied by an intriguing coupling of the excitons to the soft lattice vibrations[30–36] which controls the optical properties of 2D perovskites. The excitonic and vibrational properties can be easily tailored by an appropriate choice of organic spacers from a plethora of available molecules.[9,13,17,35,37–41] Despite the fact that the band-edge states of 2D perovskites are derived from metal and halide orbitals[14,42–44] the absorption and emission properties are affected by the octahedral templating (steric effects),[39,42,45–47] dielectric confinement[17,20] and the strength of the electron-phonon coupling.[32,35,48,49] The possibility to tune the electron-phonon coupling strength, unique for 2D perovskite semiconductors, allows to tune their emissive properties from monochromatic to white-light[11,35,50] as well as controlling the carrier cooling rate[51] and transport properties[48,52–54] crucial for any device. Although 2D perovskites have already been studied for several decades[18,55,56] many fundamental physical aspects underlying their usefulness in real devices remain to be explored. In order to fully utilize the concept of material engineering via electron-phonon coupling a detailed understanding of the complex interplay between lattice vibrations, electronic excitations and the material parameters (such as the type of organic spacer or the inorganic slab thickness) is essential.

The absorption and photoluminescence spectrum of 2D perovskites often exhibit complex shape with multiple sidebands[18,32,34,40,49,57] (see also Fig. 1 (a)-(c)). The spacing and broadening of the multiple resonances depends on the incorporated spacer molecule. For example, a dramatic increase of the resonance spacing in absorption from $\sim$ 14 to $\sim$ 40 meV can be observed when long aliphatic chains[40,57] are exchanged for spacers containing a phenyl group.[18,32,34,58,59] However the detailed mechanism leading to the appearance of these complex features is the subject of ongoing controversy. The features visible in PL and absorption spectra have been attributed to a vibronic progression[19,32,40,57,60] of excitons cou-

pled to a phonon mode of the inorganic[32,40,61] or organic[32,60] sublattice. Alternatively, it has been suggested that the complex spectrum of band-edge excitons is related to distinct excitonic transitions, the origin of which however remains to be elucidated.[18,33,34,58,59]

Here we present the results of magnetoabsorption studies of $(PEA)_2(CH_3NH_3)_{n-1}Pb_nI_{3n+1}$ for $n = 1, 2, 3$ which support the vibronic progression scenario. For all n (*i.e.* all thicknesses of the octahedral slab) we observe spectral features separated by around 40 meV in the absorption and reflectivity spectra. All the periodically spaced features exhibit identical shifts in magnetic field as expected for phonon replicas. Our results suggest the presence of a coupling between the spacer vibrations and the excitons confined in the inorganic layers for 2D Ruddlesden-Popper perovskites containing phenylethylammonium and that this coupling can be tuned by the quantum well thickness.

Fig. 1 (a)-(c) show the transmission spectra of the $n = 1$ and 2 samples together with the reflectivity contrast derivative for the $n = 3$ sample, all measured at $T = 4$ K. Transmission measurements were not possible for the $n = 3$ sample due to the large thickness of this particular crystal. The 1s excitonic transition is identified as a dominant minimum in the transmission spectrum at 2.35 eV for $n = 1$ and 2.15 eV for $n = 2$. For $n = 3$, the 1s excitonic transition can be assigned to the minimum of the derivative curve at 2.01 eV. The observed decrease of the 1s excitonic transition energies with increasing n is due to the decreasing quantum confinement, as already observed on these crystals.[62] In addition, for the $n = 1$ sample the first excited excitonic state (2s) can be identified in the transmission spectrum at around 2.5 eV. This assignment is supported by its significantly larger diamagnetic shift presented in the Supplementary Information in Fig. S1. For each sample additional features (marked by arrows in Fig. 1 (a-c)) on the higher energy side of the 1s transitions are observed. In the case of $n = 1$ two additional features with a spacing of around 40 meV are clearly visible which we assign as phonon replicas. For $n = 2$ a single phonon replica, blue-shifted by around 45 meV is visible. For $n = 3$ a weak phonon replica is observed, around 38 meV above the dominating 1s transition. The phonon energies involved (separation between 1s and phonon replica) for each n investigated are summarized in Fig. 1(d).

The results of magneto-absorption studies shown in Fig. 2 provide important information which strengthens our conclusions about the origin of the absorption side-bands. Using extreme magnetic fields up to 65 T we observe clear diamagnetic shifts of the transitions in all samples. In Fig. 2(a-c) we plot representative transmission or derivative reflectivity spectra measured at 0 and 65 T for the three samples. Despite an exciton binding energy which exceeds 200 meV,[18,20] a clear blue shift (in magnetic field) is observed which increases with increasing n. To avoid any complicated line shape analysis, the diamagnetic shift is obtained by shifting the 0T spectra to obtain perfect overlap as shown in Fig.2 (d). This works only because all features track each other perfectly in magnetic field as expected for phonon replicas. The detailed magnetic field dependence of the 1s transitions energies for all samples are presented in Fig.2 (e). In all cases the magnetic field dependence is well described by a quadratic dependence $\delta E = C_0 B^2$. The extracted diamagnetic coefficients C_0 are equal to $0.49 \pm 0.01 \mu eV/T^2$, $0.77 \pm 0.02 \mu eV/T^2$ and $1.81 \pm 0.03 \mu eV/T^2$ for $n = 1, 2, 3$ and are presented in Fig. 2(f). The diamagnetic coefficients reported for butylammonium (BA) based RP perovskites[16,40] are shown for comparison.

The increase of the diamagnetic shift with increasing n is a natural consequence of the decreasing exciton confinement and binding energy, which for $(PEA)_2(CH_3NH_3)_{n-1}Pb_nI_{n+1}$ is estimated to be 220 meV, 170 meV and 125 meV for $n = 1, 2, 3$ respectively[20] (see also Supporting Information). These diamagnetic coefficients are higher than those reported for butylammonium based RP perovskites[16] (see Fig. 2(f) which reflects the higher exciton binding energy in the latter.[55] As the diamagnetic coefficient is directly proportional to the mean square radius of the exciton wave function[63] this provides direct evidence that the excitons in PEA based 2D perovskites are

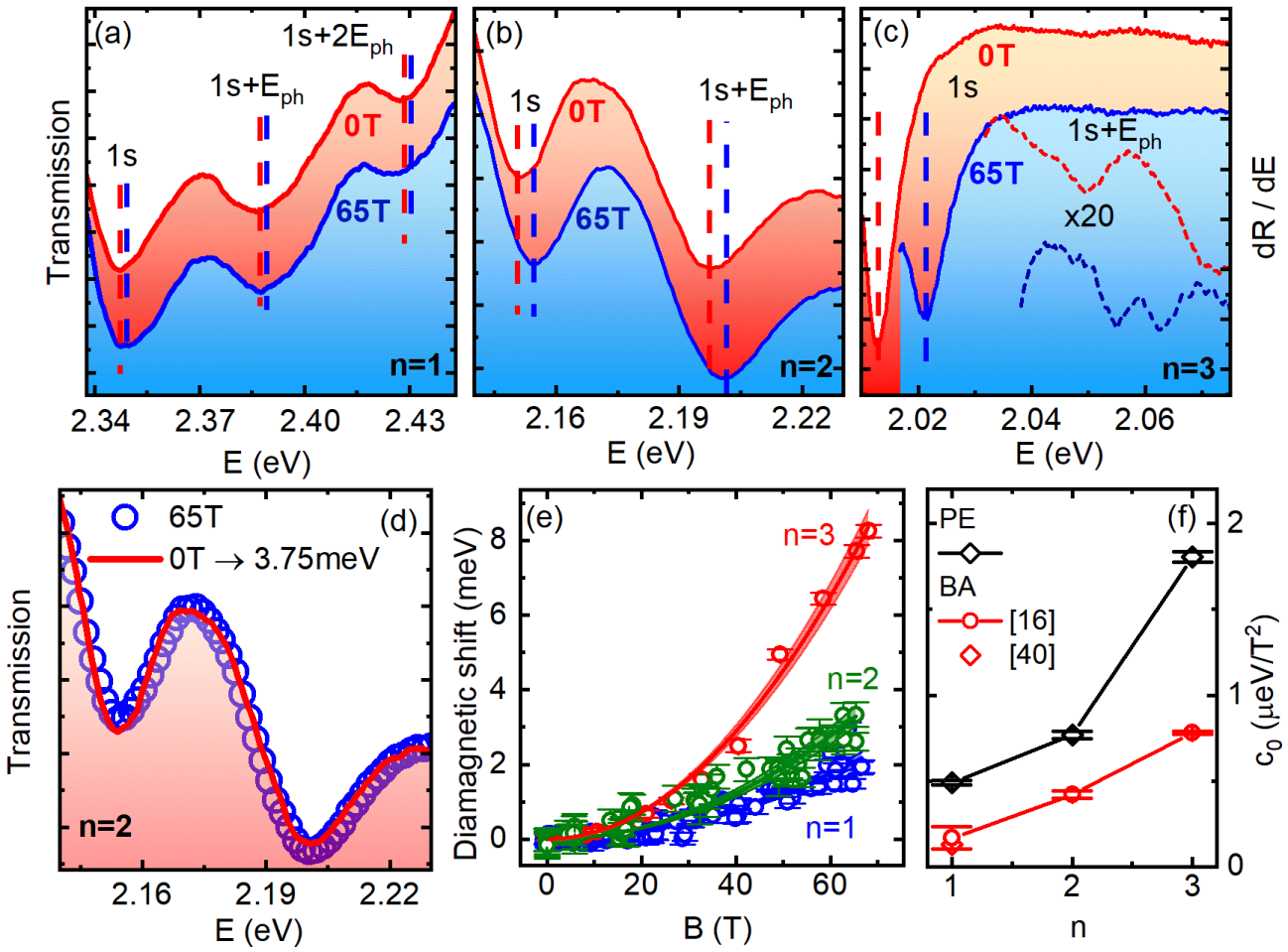

Figure 2: Transmission spectra at $T = 4\,\mathrm{K}$ in zero (red) and high magnetic field (blue) for (a) n=1 and (b) n=2 thin film samples. (c) Derivative of the reflectivity spectrum for the n=3 sample in zero (red) and high magnetic field (blue). The dashed lines in (c) show $\times 20$ magnified portions of the same derivative spectra in the higher energetic range to highlight the features at higher energies. (d) The diamagnetic shift is obtained by shifting the 0T spectra to obtain perfect overlap. Open circles are transmission spectra at 65 T, red curve is the 0 T field spectra shifted by $\sim 3.5\,\mathrm{meV}$. In addition, the perfect overlap shows that the two features exactly track each other in magnetic field. (e) Relative shifts of the 1s transitions for $n = 1, 2, 3$ as a function of the magnetic field together with quadratic fits used to obtain the diamagnetic coefficients. The shaded regions illustrate the uncertainty of the diamagnetic coefficients determined from the fits. (f) The diamagnetic coefficient of PEA (this work) and butylammonium (BA) (literature values[16,40]) as a function of the number of layers.

more spatially extended than in perovskite compounds containing alphatic chains. The larger spatial extent of the wavefunction is related to the reduced dielectric confinement induced by phenylethylammonium spacers.[20] In addition the significantly smaller out of plane corrugation of the octahedral cages in $(PEA)_2(CH_3NH_3)_{n-1}Pb_nI_{3n+1}$[64] compared to 2D perovskites with alphatic chains[65] should reduce the carrier effective mass[14,40] leading to an increased extension of the exciton wavefunction.

The origin of the complicated transmission spectrum of $(PEA)_2(CH_3NH_3)_{n-1}Pb_nI_{3n+1}$ is the subject of ongoing controversy in the literature. For $n = 1$ the high energy features separated by around 40 meV were initially attributed to phonon replicas related to the coupling of the exciton to a PEA ligand vibration.[32] Subsequently this interpretation was questioned and the observed sidebands were assigned to distinct excitons (excitons-polarons) whose detailed nature was, however, not specified.[33,34,58,59] The observation of sidebands with a similar energy spacing of around 40 meV (see Fig.1(d)) for all n is a strongly supporting argument for the interpretation that they are related to PEA ligand vibrations, more specifically to the torsional motion of the NH_3^+ head.[32,66–68] In the case of the distinct exciton-polaron pic-

ture we would rather expect significant difference in the energy separation of the additional features for different n due to the modification of quantum and dielectric confinement, analogous to the modification of the exciton binding energy and effective mass.[16] Most hypothetical mechanisms proposed in,[33] which would lead to a complex excitonic spectral structure[69–72] including spin–orbit coupling, exchange interactions or many-body correlations are highly sensitive to the octahedral layer thickness. For example the exchange interaction scales as $1/a_B^3$, where a_B is Bohr radius of the exciton.[73] Moreover, important predictions about the exciton fine structure can be derived from the orbital structure forming the band-edge states and the symmetry of the crystal. Similarly to the case of 3D perovskites, the edges of the conduction and valance bands are predominantly built from lead orbitals with total angular momentum of 1/2. The qualitative impact of spin-orbit interaction, Coulomb and exchange interaction on excitons state is well known and has already been presented and discussed in literature for 3D[74–76] and 2D perovskites.[77] In short, there are only two exciton states that couple effectively to light propagating in the direction perpendicular to the quantum well surface, which can therefore be observed in the absorption spectrum. These are states with total angular momentum $J_z = \pm 1$. Crucially, there are not enough bright exciton states to explain the complex absorption spectrum *i.e.* 3 or more absorption peaks observed in case of PEA_2PbI_4.[34,58] In addition, states which are split due to the exchange interaction behave in a characteristic way in magnetic field[74,76,78] shifting in opposite directions, leading to an increased splitting in magnetic field which is not the case here.

At the same time the energy of the organic spacer vibrations is expected to only weakly depend on the thickness of the inorganic part. Therefore, the weak variation of the energetic spacing of the transitions with n points to a common mechanism for their origin which is insensitive to the quantum well thickness. A natural candidate for such a mechanism is coupling to a phonon mode associated with the invariant organic spacer.

We would like to emphasize that we do not neglect coupling of excitons to low energy phonon modes revealed by resonant impulsive stimulated Raman spectroscopy.[33] The only issue that is in our opinion controversial is the attribution features separated by 40 meV to distinct excitonic states.

To further support this conclusion we have performed Raman scattering measurement for $(PEA)_2PbI_4$ and $(BA)_2PbI_4$ presented in Fig. 3. Here we focus on Raman modes in the spectral range around 35 meV. The spectrum of $(PEA)_2PbI_4$ displays 6 sharp modes, divided into 2 triplet-like groups, around 32 meV and 35 meV. $(BA)_2PbI_4$ n=1 spectrum displays two modes around 25 meV and 30 meV, each as wide as a triplet. The structural similarity of PEA and BA n=1, and the proximity in mode energy suggests these atomic motions are similar. Similar modes around 30 meV were also observed in the orthorhombic phase of $(CH_3NH_3)PbX_3$ (X= Cl, Br, I).[68,79] Ab initio computation of the latter, indicate that these peaks correspond to a torsional motion of the NH_3 group inside the PbX_3 cage.[32,66–68] However, the same peak was also observed in $CsPbBr_3$ where an organic molecule is absent. This suggests the peaks in this spectral range is a result of a combined motion of the A cation and the adjacent Pb-X cage.

The blue-shift in energy in PEA compared to BA is likely the result of the stronger $C-H-\pi$ interactions between the PEA molecules compared to the weak van der Waals forces between the BA molecules, which hinders the motion of NH_3 group.[80,81] The higher number of modes in PEA is due to the lower symmetry of PEA n=1 which crystallizes in a non-centrosymmetric structure (P-1) compared to the orthorhombic (Pbca) BA n=1.[49,65] The lower symmetry leads to symmetry breaking of the atomic motion involved in the specific mode as well as the breakdown of the mutual exclusion rule. This leads to the mode splitting and the observation of otherwise Raman inactive modes.[82] The energies of these Raman modes are close to the energy spacing observed in the transmission spectrum of $(PEA)_2PbI_4$ supporting our interpretation.

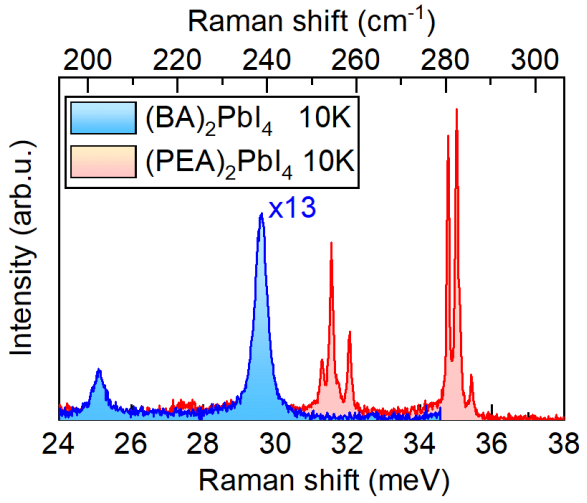

Figure 3: Raman spectrum of $(PEA)_2PbI_4$ and $(BA)_2PbI_4$ in the spectral range of 35 meV, showing the NH_3 torsional modes coupled to the exciton in $(PEA)_2PbI_4$. The intensity in the spectrum of $(BA)_2PbI_4$ was multiplied by 13 for comparison.

It is important to note that despite the fact that these high energy modes related to torsional motion of NH_3^+ are also observed in $(BA)_2PbI_4$ Raman spectrum they are absent in the excitonic spectra of this compound.[40,61,83,84] This indicates that different organic spacers, not only impose different crystal structures, but also impose different electron-phonon interactions which result in excitonic coupling to a lower energy phonon in $(BA)_2PbI_4$. Therefore, our result demonstrates that the type of organic molecule has a strong effect on the vibrational motion of the ammonium and subsequently, on the vibronic coupling.

The detailed answer why an exciton localized within the metal halide plane couples to the organic cation motion remains so far elusive. Obviously the NH_3 head penetrates the layer of octahedra and is situated below the surface of apical halide anions.[85,86] Therefore the overlap between exciton/charge density and the vibrating spacer is expected. This can explain why the intensity of the phonon replicas clearly decrease for thicker quantum wells ($n = 2, 3$). Nevertheless, the presence of coupling for PEA and absence of coupling in BA containing 2D perovskites is not obvious. It could possibly be attributed to the different nature of organic spacers molecules interaction. Alternatively we suppose that difference between BA and PEA originates from the different organic spacer interaction with apical halides by hydrogen-bonding. It was shown that it is highly sensitive to the penetration depth of the NH_3 group which has a non-trivial impact on the octahedral distortion and melting temperature.[85,86] It is possible that there exists an optimal value of the penetration depth which effectively couples the organic spacer vibration to the octahedral cages, and in this way modifies the band structure leading to exciton coupling to the NH_3 motion.

In conclusion, we have performed magneto-optical studies of 2D RP perovskites with varying octahedral slab thickness and phenylethylammonium cations as organic spacers. We demonstrate that the multiple excitonic features observed in the absorption spectra of for $n = 1, 2, 3$ can be assigned to phonon replicas of the 1s transition. This conclusion is supported by the constant energy spacing of the transitions, independent of the quantum well thickness, and their identical shift in magnetic field. Raman spectroscopy measurements reveal the presence of modes at energies corresponding to the spacing observed in the transmission spectrum which most likely give rise to the observed replicas.This indicates that the broad absorption spectrum is an inherent feature of PEA_2PbI_4 which can have direct impact on the possible applications of this material. We have also shown that the diamagnetic coefficients of the 1s transitions are higher than in the case of 2D perovskites with alkyl chain spacers which is a natural consequence of the weaker binding energy of the excitons in $(PEA)_2(CH_3NH_3)_{n-1}Pb_nI_{3n+1}$ due to the weaker dielectric confinement and different octahedral distortion.

Methods

Crystals have been synthesized following the "Anti-solvent Vapor-assisted Capping Crystallization" method[87] for $n = 1$ and 2, and by slow cooling method reported by Bakr[88] for $n = 3$. For $n = 2$, a ratio 2/0.75/1.6 of phenylethylammonium iodide, methylammonium iodide and lead iodide was used. 249 mg (1 mmol) of phenylethylammonium iodide, 59.6 mg (0.375

mmol) of methylammonium iodide and 369 mg (0.8 mmol) of lead iodide were dissolved in 1 mL of dry GBL. 10 μl of the 0.8 M solution in GBL are deposited on a cleaned quartz substrate. For $n = 3$ crystals prepared by slow cooling method, a ratio 1/24/10 of phenylamine, methylammonium and lead iodide was used. Firstly, a mixture of 2.23 g of lead oxide was dissolved in 30 mL of hydriodic acid solution (stabilized, 1.5%w H_3PO_2). Then 3.82 g of methylammonium were added and immediately dissolved. Finally, 124 μl of phenethylamine were added. The mixture was completely dissolved after 15 minutes of stirring at 80°C. The temperature was raised to 120°C for 1 hour, then the solution was slowly cooled down to room temperature at a rate of 1°C/h. The crystals were filtered and then carefully dried on paper until no trace of humidity was observed.

Transmission and reflectivity measurements were performed using a tungsten halogen lamp as a source of broad-band white light. Optical fibers were used to illuminate the sample and to collect the signal, which was dispersed by a monochromator and detected using a CCD camera. The spectral resolution of the measurement is estimated to be 0.2-0.5 meV. The measurements in magnetic field were performed in pulsed magnetic fields up to 68 T with a pulse duration of 500 ms in the Faraday configuration with the direction of the magnetic field along the out-of-plane c-axis of the layered crystals. Measurements were performed at $T = 4$ K temperature obtained by placing the sample in a helium cryostat. Ramana measurement were performed at a temperature of 10 K with excitation well below the material band gap/exciton transition provided by 785 nm laser.

Supporting Information

2s exciton states diamagnetic shift analysis, uncertainty analysis, exciton binding energy determination

Acknowledgement MB and PP appreciates support from National Science Centre Poland within the OPUS program (grant no. 2019/33/B/ST3/01915). This work was partially supported by OPEP project, which received funding from the ANR-10-LABX-0037-NEXT. Joanna M. Urban, E. Deleporte, G. Trippé-Allard and G. Chehade have received fundings from the Agence Nationale pour la Recherche, ANR-18-CE24-006 (EMIPERO). M.D. appreciates support from the Polish National Agency for Academic Exchange within the Bekker programme (grant no. PPN/BEK/2019/1/00312/U/00001).

References

(1) Tsai, H.; Nie, W.; Blancon, J.-C.; Stoumpos, C. C.; Asadpour, R.; Harutyunyan, B.; Neukirch, A. J.; Verduzco, R.; Crochet, J. J.; Tretiak, S. et al. High-efficiency two-dimensional Ruddlesden–Popper perovskite solar cells. *Nature* **2016**, *536*, 312–316.

(2) Zhang, X.; Ren, X.; Liu, B.; Munir, R.; Zhu, X.; Yang, D.; Li, J.; Liu, Y.; Smilgies, D.-M.; Li, R. et al. Stable high efficiency two-dimensional perovskite solar cells via cesium doping. *Energy Environ. Sci.* **2017**, *10*, 2095–2102.

(3) Liang, C.; Zhao, D.; Li, Y.; Li, X.; Peng, S.; Shao, G.; Xing, G. Ruddlesden–Popper Perovskite for Stable Solar Cells. *Energy & Environmental Materials* **2018**, *1*, 221–231.

(4) Smith, I. C.; Hoke, E. T.; Solis-Ibarra, D.; McGehee, M. D.; Karunadasa, H. I. A layered hybrid perovskite solar-cell absorber with enhanced moisture stability. *Angewandte Chemie International Edition* **2014**, *53*, 11232–11235.

(5) Asghar, M.; Zhang, J.; Wang, H.; Lund, P. Device stability of perovskite solar cells–A review. *Renewable and Sustainable Energy Reviews* **2017**, *77*, 131–146.

(6) Yan, J.; Qiu, W.; Wu, G.; Heremans, P.; Chen, H. Recent progress in 2D/quasi-2D layered metal halide perovskites for solar

cells. *J. Mater. Chem. A* **2018**, *6*, 11063–11077.

(7) Cao, D. H.; Stoumpos, C. C.; Farha, O. K.; Hupp, J. T.; Kanatzidis, M. G. 2D homologous perovskites as light-absorbing materials for solar cell applications. *Journal of the American Chemical Society* **2015**, *137*, 7843–7850.

(8) Blancon, J.-C.; Tsai, H.; Nie, W.; Stoumpos, C. C.; Pedesseau, L.; Katan, C.; Kepenekian, M.; Soe, C. M. M.; Appavoo, K.; Sfeir, M. Y. et al. Extremely efficient internal exciton dissociation through edge states in layered 2D perovskites. *Science* **2017**, *355*, 1288–1292.

(9) Yang, R.; Li, R.; Cao, Y.; Wei, Y.; Miao, Y.; Tan, W. L.; Jiao, X.; Chen, H.; Zhang, L.; Chen, Q. et al. Oriented Quasi-2D Perovskites for High Performance Optoelectronic Devices. *Advanced Materials* **2018**, *30*, 1804771.

(10) Brehier, A.; Parashkov, R.; Lauret, J. S.; Deleporte, E. Strong exciton-photon coupling in a microcavity containing layered perovskite semiconductors. *Applied Physics Letters* **2006**, *89*, 171110.

(11) Gong, X.; Voznyy, O.; Jain, A.; Liu, W.; Sabatini, R.; Piontkowski, Z.; Walters, G.; Bappi, G.; Nokhrin, S.; Bushuyev, O. et al. Electron–phonon interaction in efficient perovskite blue emitters. *Nature materials* **2018**, *17*, 550–556.

(12) Vashishtha, P.; Ng, M.; Shivarudraiah, S. B.; Halpert, J. E. High Efficiency Blue and Green Light-Emitting Diodes Using Ruddlesden–Popper Inorganic Mixed Halide Perovskites with Butylammonium Interlayers. *Chemistry of Materials* **2019**, *31*, 83–89.

(13) Chen, Y.; Sun, Y.; Peng, J.; Tang, J.; Zheng, K.; Liang, Z. 2D Ruddlesden–Popper perovskites for optoelectronics. *Advanced Materials* **2018**, *30*, 1703487.

(14) Pedesseau, L.; Sapori, D.; Traore, B.; Robles, R.; Fang, H.-H.; Loi, M. A.; Tsai, H.; Nie, W.; Blancon, J.-C.; Neukirch, A. et al. Advances and promises of layered halide hybrid perovskite semiconductors. *ACS nano* **2016**, *10*, 9776–9786.

(15) Even, J.; Pedesseau, L.; Katan, C. Understanding quantum confinement of charge carriers in layered 2D hybrid perovskites. *ChemPhysChem* **2014**, *15*, 3733–3741.

(16) Blancon, J.-C.; Stier, A. V.; Tsai, H.; Nie, W.; Stoumpos, C. C.; Traoré, B.; Pedesseau, L.; Kepenekian, M.; Katsutani, F.; Noe, G. T. et al. Scaling law for excitons in 2D perovskite quantum wells. *Nature Communications* **2018**, *9*, 2254.

(17) Straus, D. B.; Kagan, C. R. Electrons, excitons, and phonons in two-dimensional hybrid perovskites: connecting structural, optical, and electronic properties. *The journal of physical chemistry letters* **2018**, *9*, 1434–1447.

(18) Gauthron, K.; Lauret, J.-S.; Doyennette, L.; Lanty, G.; Choueiry, A. A.; Zhang, S.; Brehier, A.; Largeau, L.; Mauguin, O.; Bloch, J. et al. Optical spectroscopy of two-dimensional layered $(C_6H_5C_2H_4\text{-}NH_3)_2\text{-}PbI_4$ perovskite. *Opt. Express* **2010**, *18*, 5912–5919.

(19) Tanaka, K.; Takahashi, T.; Kondo, T.; Umebayashi, T.; Asai, K.; Ema, K. Image charge effect on two-dimensional excitons in an inorganic-organic quantum-well crystal. *Physical Review B* **2005**, *71*, 045312.

(20) Ishihara, T.; Hong, X.; Ding, J.; Nurmikko, A. V. Dielectric confinement effect for exciton and biexciton states in PbI4-based two-dimensional semiconductor structures. *Surface Science* **1992**, *267*, 323 – 326.

(21) Hong, X.; Ishihara, T.; Nurmikko, A. Dielectric confinement effect on excitons

in PbI 4-based layered semiconductors. *Physical Review B* **1992**, *45*, 6961.

(22) Byun, J.; Cho, H.; Wolf, C.; Jang, M.; Sadhanala, A.; Friend, R. H.; Yang, H.; Lee, T.-W. Efficient Visible Quasi-2D Perovskite Light-Emitting Diodes. *Advanced Materials* **2016**, *28*, 7515–7520.

(23) Jia, G.; Shi, Z.-J.; Xia, Y.-D.; Wei, Q.; Chen, Y.-H.; Xing, G.-C.; Huang, W. Super air stable quasi-2D organic-inorganic hybrid perovskites for visible light-emitting diodes. *Opt. Express* **2018**, *26*, A66–A74.

(24) Fieramosca, A.; Polimeno, L.; Ardizzone, V.; De Marco, L.; Pugliese, M.; Maiorano, V.; De Giorgi, M.; Dominici, L.; Gigli, G.; Gerace, D. et al. Two-dimensional hybrid perovskites sustaining strong polariton interactions at room temperature. *Science Advances* **2019**, *5*.

(25) Ugeda, M. M.; Bradley, A. J.; Shi, S.-F.; da Jornada, F. H.; Zhang, Y.; Qiu, D. Y.; Ruan, W.; Mo, S.-K.; Hussain, Z.; Shen, Z.-X. et al. Giant bandgap renormalization and excitonic effects in a monolayer transition metal dichalcogenide semiconductor. *Nature Materials* **2014**, *13*, 1091–1095.

(26) Goryca, M.; Li, J.; Stier, A. V.; Taniguchi, T.; Watanabe, K.; Courtade, E.; Shree, S.; Robert, C.; Urbaszek, B.; Marie, X. et al. Revealing exciton masses and dielectric properties of monolayer semiconductors with high magnetic fields. *Nature communications* **2019**, *10*, 1–12.

(27) Chernikov, A.; Berkelbach, T. C.; Hill, H. M.; Rigosi, A.; Li, Y.; Aslan, O. B.; Reichman, D. R.; Hybertsen, M. S.; Heinz, T. F. Exciton binding energy and nonhydrogenic Rydberg series in monolayer WS 2. *Physical review letters* **2014**, *113*, 076802.

(28) Tran, V.; Soklaski, R.; Liang, Y.; Yang, L. Layer-controlled band gap and anisotropic excitons in few-layer black phosphorus. *Physical Review B* **2014**, *89*, 235319.

(29) Wang, X.; Jones, A. M.; Seyler, K. L.; Tran, V.; Jia, Y.; Zhao, H.; Wang, H.; Yang, L.; Xu, X.; Xia, F. Highly anisotropic and robust excitons in monolayer black phosphorus. *Nature nanotechnology* **2015**, *10*, 517–521.

(30) Meggiolaro, D.; Ambrosio, F.; Mosconi, E.; Mahata, A.; De Angelis, F. Polarons in Metal Halide Perovskites. *Advanced Energy Materials* **2019**, 1902748.

(31) Mao, L.; Wu, Y.; Stoumpos, C. C.; Wasielewski, M. R.; Kanatzidis, M. G. White-light emission and structural distortion in new corrugated two-dimensional lead bromide perovskites. *Journal of the American Chemical Society* **2017**, *139*, 5210–5215.

(32) Straus, D. B.; Parra, S. H.; Iotov, N.; Gebhardt, J.; Rappe, A. M.; Subotnik, J. E.; Kikkawa, J. M.; Kagan, C. R. Direct Observation of Electron-Phonon Coupling and Slow Vibrational Relaxation in Organic-Inorganic Hybrid Perovskites. *J. Am. Chem. Soc.* **2016**, 4.

(33) Thouin, F.; Valverde-Chávez, D. A.; Quarti, C.; Cortecchia, D.; Bargigia, I.; Beljonne, D.; Petrozza, A.; Silva, C.; Srimath Kandada, A. R. Phonon coherences reveal the polaronic character of excitons in two-dimensional lead halide perovskites. *Nature Materials* **2019**, *18*, 349–356.

(34) Neutzner, S.; Thouin, F.; Cortecchia, D.; Petrozza, A.; Silva, C.; Srimath Kandada, A. R. Exciton-polaron spectral structures in two-dimensional hybrid lead-halide perovskites. *Phys. Rev. Materials* **2018**, *2*, 064605.

(35) Smith, M. D.; Karunadasa, H. I. White-light emission from layered halide perovskites. *Accounts of chemical research* **2018**, *51*, 619–627.

(36) Zhang, S.-F.; Chen, X.-K.; Ren, A.-M.; Li, H.; Bredas, J.-L. Impact of Organic Spacers on the Carrier Dynamics in 2D Hybrid Lead-Halide Perovskites. *ACS Energy Letters* **2018**, *4*, 17–25.

(37) Jiang, J.; Pachter, R.; Lim, C.-K.; Haley, J. E.; Prasad, P. N. Elucidating the Role of the Organic Cation in Tuning the Optical Response of Two-Dimensional Organic–Inorganic Halide Perovskites by Computational Investigation. *The Journal of Physical Chemistry C* **2020**, *124*, 3224–3232.

(38) Ishihara, T. Optical properties of PbI-based perovskite structures. *Journal of Luminescence* **1994**, *60-61*, 269–274.

(39) Sourisseau, S.; Louvain, N.; Bi, W.; Mercier, N.; Rondeau, D.; Boucher, F.; Buzaré, J.-Y.; Legein, C. Reduced Band Gap Hybrid Perovskites Resulting from Combined Hydrogen and Halogen Bonding at the Organic-Inorganic Interface. *Chemistry of Materials* **2007**, *19*, 600–607.

(40) Baranowski, M.; Zelewski, S. J.; Kepenekian, M.; Traoré, B.; Urban, J. M.; Surrente, A.; Galkowski, K.; Maude, D. K.; Kuc, A.; Booker, E. P. et al. Phase-Transition-Induced Carrier Mass Enhancement in 2D Ruddlesden–Popper Perovskites. *ACS Energy Letters* **2019**, *4*, 2386–2392.

(41) Chen, S.; Shen, N.; Zhang, L.; Zhang, L.; Cheung, S. H.; Chen, S.; So, S. K.; Xu, B. Understanding the Interplay of Binary Organic Spacer in Ruddlesden–Popper Perovskites toward Efficient and Stable Solar Cells. *Advanced Functional Materials* **2020**, *30*, 1907759.

(42) Knutson, J. L.; Martin, J. D.; Mitzi, D. B. Tuning the Band Gap in Hybrid Tin Iodide Perovskite Semiconductors Using Structural Templating. *Inorganic Chemistry* **2005**, *44*, 4699–4705.

(43) Stoumpos, C. C.; Cao, D. H.; Clark, D. J.; Young, J.; Rondinelli, J. M.; Jang, J. I.; Hupp, J. T.; Kanatzidis, M. G. Ruddlesden–Popper Hybrid Lead Iodide Perovskite 2D Homologous Semiconductors. *Chemistry of Materials* **2016**, *28*, 2852–2867.

(44) Tao, S.; Schmidt, I.; Brocks, G.; Jiang, J.; Tranca, I.; Meerholz, K.; Olthof, S. Absolute energy level positions in tin- and lead-based halide perovskites. *Nature Communications* **2019**, *10*, 2560.

(45) Mercier, N.; Poiroux, S.; Riou, A.; Batail, P. Unique Hydrogen Bonding Correlating with a Reduced Band Gap and Phase Transition in the Hybrid Perovskites $(HO(CH_2)_2NH_3)_2PbX_4$ (X = I, Br). *Inorganic Chemistry* **2004**, *43*, 8361–8366.

(46) Tian, C.; Liang, Y.; Chen, W.; Huang, Y.; Huang, X.; Tian, F.; Yang, X. Hydrogen-bond enhancement triggered structural evolution and band gap engineering of hybrid perovskite $(C_6H_5CH_2NH_3)_2PbI_4$ under high pressure. *Phys. Chem. Chem. Phys.* **2020**, *22*, 1841–1846.

(47) Sharma, R.; Dai, Z.; Gao, L.; Brenner, T. M.; Yadgarov, L.; Zhang, J.; Rakita, Y.; Korobko, R.; Rappe, A. M.; Yaffe, O. By process of illumination: Revealing the causes of dramatic anharmonicity in $CH_3NH_3PbI_3$ with Raman scattering. 2020.

(48) Seitz, M.; Magdaleno, A. J.; Alcázar-Cano, N.; Meléndez, M.; Lubbers, T. J.; Walraven, S. W.; Pakdel, S.; Prada, E.; Delgado-Buscalioni, R.; Prins, F. Exciton diffusion in two-dimensional metal-halide perovskites. **2020**, arXiv:2001.05704 [physics.app-ph].

(49) Straus, D. B.; Iotov, N.; Gau, M. R.; Zhao, Q.; Carroll, P. J.; Kagan, C. R. Longer cations increase energetic disorder in excitonic 2D hybrid perovskites. *The*

journal of physical chemistry letters **2019**, *10*, 1198–1205.

(50) Cortecchia, D.; Yin, J.; Bruno, A.; Lo, S.-Z. A.; Gurzadyan, G. G.; Mhaisalkar, S.; Brédas, J.-L.; Soci, C. Polaron self-localization in white-light emitting hybrid perovskites. *J. Mater. Chem. C* **2017**, *5*, 2771–2780.

(51) Yin, J.; Maity, P.; Naphade, R.; Cheng, B.; He, J.-H.; Bakr, O. M.; Brédas, J.-L.; Mohammed, O. F. Tuning Hot Carrier Cooling Dynamics by Dielectric Confinement in Two-Dimensional Hybrid Perovskite Crystals. *ACS Nano* **2019**, *13*, 12621–12629.

(52) Zhu, X.-Y.; Podzorov, V. Charge Carriers in Hybrid Organic–Inorganic Lead Halide Perovskites Might Be Protected as Large Polarons. *The Journal of Physical Chemistry Letters* **2015**, *6*, 4758–4761.

(53) Zhu, H.; Miyata, K.; Fu, Y.; Wang, J.; Joshi, P. P.; Niesner, D.; Williams, K. W.; Jin, S.; Zhu, X.-Y. Screening in crystalline liquids protects energetic carriers in hybrid perovskites. *Science* **2016**, *353*, 1409–1413.

(54) Deng, S.; Shi, E.; Yuan, L.; Jin, L.; Dou, L.; Huang, L. Long-range exciton transport and slow annihilation in two-dimensional hybrid perovskites. *Nature Communications* **2020**, *11*, 1–8.

(55) Ishihara, T.; Takahashi, J.; Goto, T. Exciton State In Two-Dimensional Perovskite Semiconductor $(C_{10}H_{21}NH_3)_2PbI_4$. *Solid State Communications* **1989**, *69*, 4.

(56) Mitzi, D. B. Synthesis, Crystal Structure, and Optical and Thermal Properties of $(C_4H_9NH_3)_2MI_4$(M = Ge, Sn, Pb). *Chemistry of Materials* **1996**, *8*, 791–800.

(57) Kataoka, T.; Kondo, T.; Ito, R.; Sasaki, S.; Uchida, K.; Miura, N. Magneto-optical study on excitonic spectra in $(C_6H_{13}NH_3)_2PbI_4$. *Physical Review B* **1993**, *47*, 2010–2018.

(58) Kandada, A. R. S.; Silva, C. Perspective: Exciton polarons in two-dimensional hybrid metal-halide perovskites. *arXiv preprint arXiv:1908.03909* **2019**,

(59) Thouin, F.; Cortecchia, D.; Petrozza, A.; Kandada, A. R. S.; Silva, C. Enhanced screening and spectral diversity in many-body elastic scattering of excitons in two-dimensional hybrid metal-halide perovskites. *Physical Review Research* **2019**, *1*, 032032.

(60) Straus, D. B.; Hurtado-Parra, S.; Iotov, N.; Zhao, Q.; Gau, M. R.; Carroll, P. J.; Kikkawa, J. M.; Kagan, C. R. Tailoring Hot Exciton Dynamics in 2D Hybrid Perovskites through Cation Modification. *arXiv preprint arXiv:2001.03009* **2020**,

(61) Mauck, C. M.; France-Lanord, A.; Hernandez Oendra, A. C.; Dahod, N. S.; Grossman, J. C.; Tisdale, W. A. Inorganic Cage Motion Dominates Excited-State Dynamics in 2D-Layered Perovskites $(C_xH_{2x+1}NH_3)_2PbI_4$ (x = 4–9). *The Journal of Physical Chemistry C* **2019**, *123*, 27904–27916.

(62) Delport, G.; Chehade, G.; Lédée, F.; Diab, H.; Milesi-Brault, C.; Trippé-Allard, G.; Even, J.; Lauret, J.-S.; Deleporte, E.; Garrot, D. Exciton–Exciton Annihilation in Two-Dimensional Halide Perovskites at Room Temperature. *The Journal of Physical Chemistry Letters* **2019**, *10*, 5153–5159.

(63) Stier, A. V.; Wilson, N. P.; Velizhanin, K. A.; Kono, J.; Xu, X.; Crooker, S. A. Magnetooptics of Exciton Rydberg States in a Monolayer Semiconductor. *Phys. Rev. Lett.* **2018**, *120*, 057405.

(64) Calabrese, J.; Jones, N. L.; Harlow, R. L.; Herron, N.; Thorn, D. L.; Wang, Y. Preparation and Characterization of Layered Lead Halide Compounds. *Journal of the*

American Chemical Society **1991**, *113*, 2328–2330.

(65) Billing, D. G.; Lemmerer, A. Synthesis, characterization and phase transitions in the inorganic–organic layered perovskite-type hybrids $[(C_nH_{2n+1}NH_3)_2PbI_4]$, n = 4, 5 and 6. *Acta Crystallographica Section B: Structural Science* **2007**, *63*, 735–747.

(66) Brivio, F.; Frost, J. M.; Skelton, J. M.; Jackson, A. J.; Weber, O. J.; Weller, M. T.; Goni, A. R.; Leguy, A. M.; Barnes, P. R.; Walsh, A. Lattice dynamics and vibrational spectra of the orthorhombic, tetragonal, and cubic phases of methylammonium lead iodide. *Physical Review B* **2015**, *92*, 144308.

(67) Ivanovska, T.; Quarti, C.; Grancini, G.; Petrozza, A.; De Angelis, F.; Milani, A.; Ruani, G. Vibrational response of methylammonium lead iodide: From cation dynamics to phonon–phonon interactions. *ChemSusChem* **2016**, *9*, 2994–3004.

(68) Leguy, A. M. A.; Goñi, A. R.; Frost, J. M.; Skelton, J.; Brivio, F.; Rodríguez-Martínez, X.; Weber, O. J.; Pallipurath, A.; Alonso, M. I.; Campoy-Quiles, M. et al. Dynamic disorder, phonon lifetimes, and the assignment of modes to the vibrational spectra of methylammonium lead halide perovskites. *Phys. Chem. Chem. Phys.* **2016**, *18*, 27051–27066.

(69) Zhai, Y.; Baniya, S.; Zhang, C.; Li, J.; Haney, P.; Sheng, C.-X.; Ehrenfreund, E.; Vardeny, Z. V. Giant Rashba splitting in 2D organic-inorganic halide perovskites measured by transient spectroscopies. *Science Advances* **2017**, *3*.

(70) Liu, X.; Chanana, A.; Huynh, U.; Xue, F.; Haney, P.; Blair, S.; Jiang, X.; Vardeny, Z. V. Circular photogalvanic spectroscopy of Rashba splitting in 2D hybrid organic-inorganic perovskite multiple quantum wells. *Nature Communications* **2020**, *11*, 323.

(71) Tamarat, P.; Bodnarchuk, M. I.; Trebbia, J.-B.; Erni, R.; Kovalenko, M. V.; Even, J.; Lounis, B. The ground exciton state of formamidinium lead bromide perovskite nanocrystals is a singlet dark state. *Nature Materials* **2019**, *18*, 717–724.

(72) Kato, Y.; Ichii, D.; Ohashi, K.; Kunugita, H.; Ema, K.; Tanaka, K.; Takahashi, T.; Kondo, T. Extremely large binding energy of biexcitons in an organic–inorganic quantum-well material $(C_4H_9NH_3)_2PbBr_4$. *Solid State Communications* **2003**, *128*, 15 – 18.

(73) Fu, H.; Wang, L.-W.; Zunger, A. Excitonic exchange splitting in bulk semiconductors. *Physical Review B* **1999**, *59*, 5568.

(74) Fu, M.; Tamarat, P.; Huang, H.; Even, J.; Rogach, A. L.; Lounis, B. Neutral and charged exciton fine structure in single lead halide perovskite nanocrystals revealed by magneto-optical spectroscopy. *Nano letters* **2017**, *17*, 2895–2901.

(75) Ramade, J.; Andriambariarijaona, L. M.; Steinmetz, V.; Goubet, N.; Legrand, L.; Barisien, T.; Bernardot, F.; Testelin, C.; Lhuillier, E.; Bramati, A. et al. Fine structure of excitons and electron–hole exchange energy in polymorphic CsPbBr 3 single nanocrystals. *Nanoscale* **2018**, *10*, 6393–6401.

(76) Baranowski, M.; Galkowski, K.; Surrente, A.; Urban, J.; Kłopotowski, Ł.; Mackowski, S.; Maude, D. K.; Ben Aich, R.; Boujdaria, K.; Chamarro, M. et al. Giant Fine Structure Splitting of the Bright Exciton in a Bulk MAPbBr3 Single Crystal. *Nano letters* **2019**, *19*, 7054–7061.

(77) Tanaka, K.; Takahashi, T.; Kondo, T.; Umeda, K.; Ema, K.; Umebayashi, T.; Asai, K.; Uchida, K.; Miura, N. Electronic and excitonic structures of inorganic–organic perovskite-type quantum-well crystal (C4H9NH3) 2PbBr4. *Japanese journal of applied physics* **2005**, *44*, 5923.

(78) Bayer, M.; Ortner, G.; Stern, O.; Kuther, A.; Gorbunov, A.; Forchel, A.; Hawrylak, P.; Fafard, S.; Hinzer, K.; Reinecke, T. et al. Fine structure of neutral and charged excitons in self-assembled In (Ga) As/(Al) GaAs quantum dots. *Physical Review B* **2002**, *65*, 195315.

(79) Nakada, K.; Matsumoto, Y.; Shimoi, Y.; Yamada, K.; Furukawa, Y. Temperature-dependent evolution of Raman spectra of methylammonium lead halide perovskites, $CH_3NH_3PbX_3$ (X = I, Br). *Molecules* **2019**, *24*.

(80) Mitzi, D. B. Synthesis, structure, and properties of organic-inorganic perovskites and related materials. *Progress in inorganic chemistry* **1999**, 1–121.

(81) Saparov, B.; Mitzi, D. B. Organic–inorganic perovskites: structural versatility for functional materials design. *Chemical reviews* **2016**, *116*, 4558–4596.

(82) Bhagavantam, S.; Venkatarayudu, T. Raman effect in relation to crystal structure. Proceedings of the Indian Academy of Sciences-Section A. 1939; pp 224–258.

(83) Ni, L.; Huynh, U.; Cheminal, A.; Thomas, T. H.; Shivanna, R.; Hinrichsen, T. F.; Ahmad, S.; Sadhanala, A.; Rao, A. Real-time observation of exciton–phonon coupling dynamics in self-assembled hybrid perovskite quantum wells. *ACS nano* **2017**, *11*, 10834–10843.

(84) Sichert, J. A.; Hemmerling, A.; Cardenas-Daw, C.; Urban, A. S.; Feldmann, J. Tuning the optical bandgap in layered hybrid perovskites through variation of alkyl chain length. *APL Materials* **2019**, *7*, 041116.

(85) Du, K.-z.; Tu, Q.; Zhang, X.; Han, Q.; Liu, J.; Zauscher, S.; Mitzi, D. B. Two-dimensional lead (II) halide-based hybrid perovskites templated by acene alkylamines: Crystal structures, optical properties, and piezoelectricity. *Inorganic chemistry* **2017**, *56*, 9291–9302.

(86) Li, T.; Dunlap-Shohl, W. A.; Reinheimer, E. W.; Le Magueres, P.; Mitzi, D. B. Melting temperature suppression of layered hybrid lead halide perovskites via organic ammonium cation branching. *Chemical science* **2019**, *10*, 1168–1175.

(87) Lédée, F.; Trippé-Allard, G.; Diab, H.; Audebert, P.; Garrot, D.; Lauret, J.-S.; Deleporte, E. Fast growth of monocrystalline thin films of 2D layered hybrid perovskite. *CrystEngComm* **2017**, *19*, 2598–2602.

(88) Peng, W.; Yin, J.; Ho, K.-T.; Ouellette, O.; De Bastiani, M.; Murali, B.; El Tall, O.; Shen, C.; Miao, X.; Pan, J. et al. Ultralow Self-Doping in Two-dimensional Hybrid Perovskite Single Crystals. *Nano Letters* **2017**, *17*, 4759–4767.